JOURNAL OF AIRCRAFT
Vol. 36, No. 4, July–August 1999

Numerical Optimization of Fuselage Geometry to Modify Sonic-Boom Signature

Yoshikazu Makino,* Takashi Aoyama,† and Toshiyuki Iwamiya‡
National Aerospace Laboratory, Tokyo 182-8522, Japan
and
Tadaharu Watanuki§ and Hirotoshi Kubota¶
University of Tokyo, Tokyo 113-8656, Japan

A low-sonic-boom design method is developed by combining a three-dimensional Euler computational fluid dynamics code with a least-squares optimization technique. In this design method, the fuselage geometry of an aircraft is modified to minimize the pressure discrepancies between a target low-boom pressure signature and a calculated signature. The aircraft configurations that generate three types of low-boom pressure signatures, i.e., flattop type, ramp type, and hybrid type, are successfully designed by this method. It is shown that the sonic-boom intensity of the aircraft designed by linear theory is reduced and the flattop-type ground pressure signature is obtained by this method. The results of the study suggest that this method is a useful tool for low-boom design.

Nomenclature

A_e = equivalent-area distribution of aircraft
C_{Dp} = pressure drag coefficient
C_L = lift coefficient
$F(\tau)$ = F function
H = normal distance from aircraft
J = object function in optimization process
K = number of design variables used in optimization process
L = aircraft length
M = freestream Mach number
P_b = baseline pressure in optimization process
P_t = target pressure in optimization process
p_∞ = freestream static pressure
x = streamwise location
y = spanwise location
β = $\sqrt{M^2-1}$
γ = specific heat ratio
Δp = shock overpressure
ΔS = element length of pressure signature
ΔT_R = rise time of shock overpressure
δ_k = kth design variable

Subscript

i = ith element of pressure signature in optimization process

Introduction

THE sonic boom caused by supersonic overland flight is one of the biggest environmental problems for the supersonic transport (SST). A lot of prediction methods for the sonic boom have been already developed. Whitham[1] developed a modified linear theory called the F-function method. This method was originally applicable for only a body of revolution, but it was extended for a wing body later by Walkden.[2] Thomas[3] presented a computational method to extrapolate a near-field pressure signature out to the far field, which is called the waveform parameter method. The F-function method and the waveform parameter method are mathematically equivalent because both methods utilize geometric acoustics and isentropic wave theory. The waveform parameter method needs a near-field pressure signature as input data. Computational fluid dynamics (CFD) is one suitable approach to simulate the near-field pressure signature[4,5] because it is applicable to cases that include strong shock waves. In this study, a finite-difference Euler code is used to predict the near-field pressure signature and the waveform parameter method is applied to extrapolate the near-field pressure signature to the ground.

Many kinds of methods to reduce the sonic-boom intensity have been published. Seebass and George[6] determined the area distribution that minimized the sonic-boom intensity. However, the area distribution has an extremely blunt nose shape that produces large drag. Darden[7] modified this minimization method in order to reduce the drag by controlling the bluntness of the area distribution near the nose. Compared with these low-boom design methods based on linear theory, a low-boom design method for which numerical optimization is used is presented in this study.

Low-Boom Design Method Based on Linear Theory

Figure 1 shows the concept of Darden's low-boom design.[7] This method is based on the F-function method. In the F-function method, the perturbation pressure is given by

$$\frac{p-p_\infty}{p_\infty}=\frac{\gamma M^2}{\sqrt{2\beta(H/L)}}F(\tau) \tag{1}$$

The F function $F(\tau)$ can be expressed as

$$F(\tau)=\frac{1}{2\pi}\int_0^\tau \frac{Ae''}{\sqrt{\tau-t}}\,\mathrm{d}t \tag{2}$$

In Darden's low-boom design method, the F function is defined by several parameters, shown in Fig. 1, and each parameter has an influence on the shape of the ground pressure signature or the sonic-boom intensity. Figure 2 shows three types of low-boom pressure signatures: a flattop-type, a ramp-type, and a hybrid-type pressure signature. Darden's low-boom design method can consider the first

Received 8 July 1998; revision received 26 February 1999; accepted for publication 28 February 1999.

*Researcher, Advanced Technology Aircraft Project Center, 7-44-1 Jindaiji-higashi, Chofu. Member AIAA.
†Senior Researcher, Fluid Science Research Center, 7-44-1 Jindaiji-higashi, Chofu. Member AIAA.
‡Head, Computational Science Division, 7-44-1 Jindaiji-higashi, Chofu.
§Research Assistant, Department of Aeronautics and Astronautics, 7-3-1 Hongo, Bunkyo.
¶Professor, Department of Aeronautics and Astronautics, 7-3-1 Hongo, Bunkyo. Associate Fellow AIAA.

Table 1 Aircraft dimensions and flight conditions

Aircraft length	91.4 m
Weight	3175 tons
Wing planform area	1115 m^2
Design Mach number	1.4
Flight altitude	12.8 km

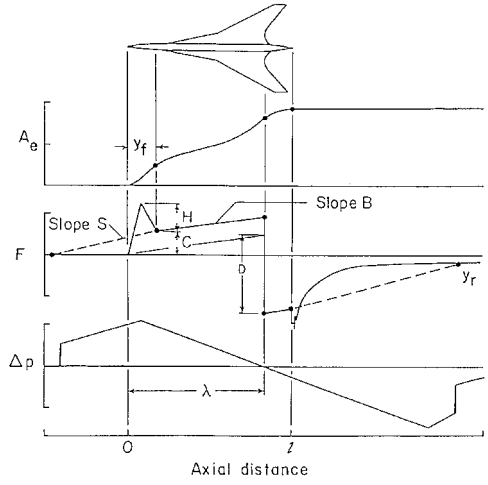

Fig. 1 Concept of low-boom design.[7]

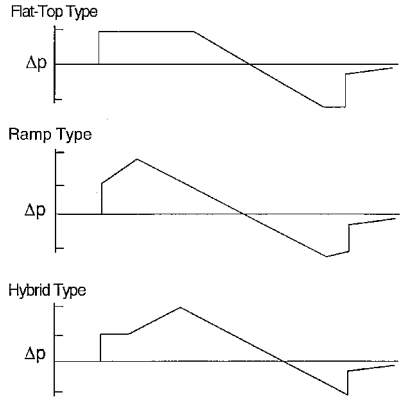

Fig. 2 Low-boom pressure signatures.

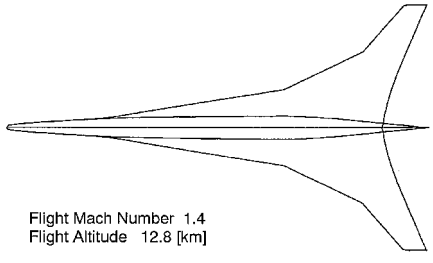

Fig. 3 Low-boom configuration.[8]

two types. A flattop-type pressure signature is generated when parameter B in Fig. 1 is 0.0, and a ramp-type pressure signature is generated when B has a positive value. The F function shown in Fig. 1 has a spiked part in the nose region, and the parameter y_f is the width of the spiked part. This parameter controls the nose bluntness of the aircraft. The aircraft has a blunt nose when y_f is small.

The sonic-boom intensity of the low-boom aircraft configuration[8] (Fig. 3) designed by Darden's method was predicted in our previous study.[9] The dimensions of this aircraft and flight conditions are shown in Table 1. Darden's low-boom design method provides only the total equivalent-area distribution, which consists of two basic components: the actual area of the configuration and the equivalent area that is due to the distribution of lift. The actual area at a given point on the flight-path axis is determined by a frontal projection of the body component areas intercepted by a cutting plane inclined at a Mach angle with respect to the body axis. The equivalent area that is due to the distribution of lift is determined by a summation of a local force per unit longitudinal distance. Therefore infinite combinations of fuselage and wing geometry that have the same total equivalent-area distribution are possible. In the case of this low-boom aircraft configuration, the wing planform is first determined by a supersonic theory for drag reduction and the wing is warped to reduce induced drag. The fuselage geometry is next determined for boom minimization. The configuration is designed to generate a flattop-type pressure signature on the ground by Darden's theory. The initial peak pressure level estimated by linear theory is 42 Pa. The value of the parameter y_f/L for this configuration is set at 0.00001, which means a blunt nose.

The near-field pressure signature for the low-boom configuration is obtained with a fully three-dimensional Euler code. The numerical method used to solve the governing equations is an implicit finite-difference scheme. The diagonalized alternative-direction-implicit scheme, which utilizes an upwind flux-split technique, is used for the implicit left-hand side. In addition, a higher-order upwind scheme based on the total-variation-diminishing scheme by Chakravarthy and Osher[10] is applied to the inviscid terms of the explicit right-hand side. This numerical code has been used to calculate near-field pressure signatures of several SST configurations in Refs. 9 and 11. The calculated near-field pressure signatures showed good agreement with experimental data. The computational grid generated around the low-boom configuration is shown in Fig. 4. It is generated by stacking two-dimensional plane grids that are normal to the body axis. The grid outer boundary and the downstream grid surface are extended outward from the body axis in order to capture shock waves sharply at some distance from the aircraft. Figure 5 shows the calculated near-field pressure signatures for this low-boom configuration. In the nose region of the signature, a spiked part that is a feature of the low-boom pressure signature is shown at $H/L = 1.0$, and this spiked part becomes a flattop shape at $H/L = 6.0$. In the rear part of the signature, some pressure peaks are shown at $H/L = 1.0$. The highest-pressure peak of them is due to the strong shocks from the outer-wing leading edges. These peaks coalesce into one high-pressure peak as the distance from the aircraft becomes large.

Figure 6 shows the equivalent-area distributions of the low-boom configuration. In this figure, Volume and Lift mean the actual area of the configuration and the equivalent area that is due to the distribution of lift calculated from the CFD result, respectively. The total equivalent-area distribution, which is a summation of the above two components, and the equivalent-area distribution designed by Darden's method are represented by Volume + Lift and Designed,

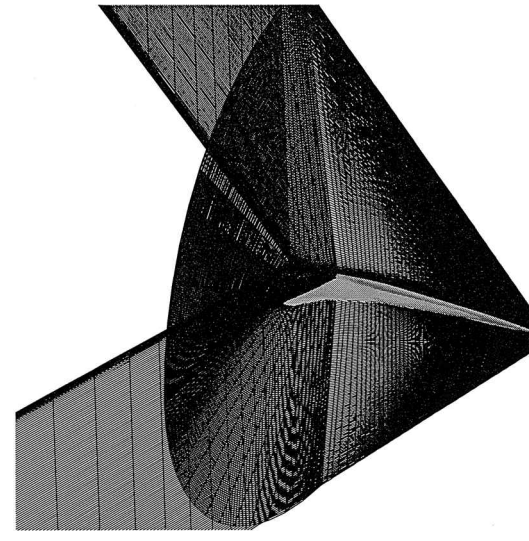

Fig. 4 Computational grid (53 × 130 × 140).

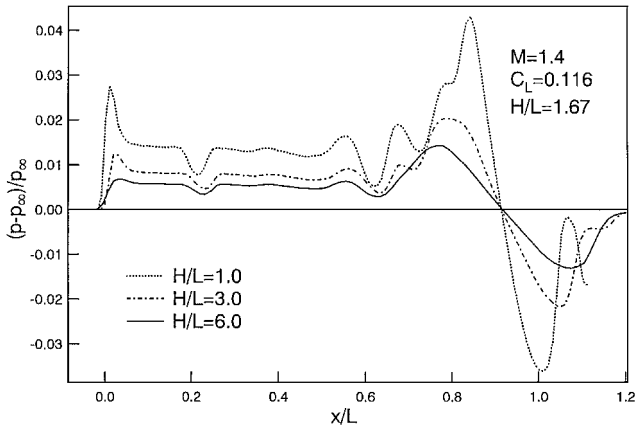

Fig. 5 Calculated near-field pressure signatures.

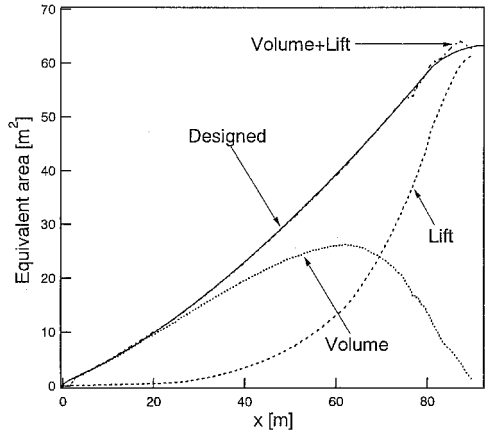

Fig. 6 Equivalent-area distributions.

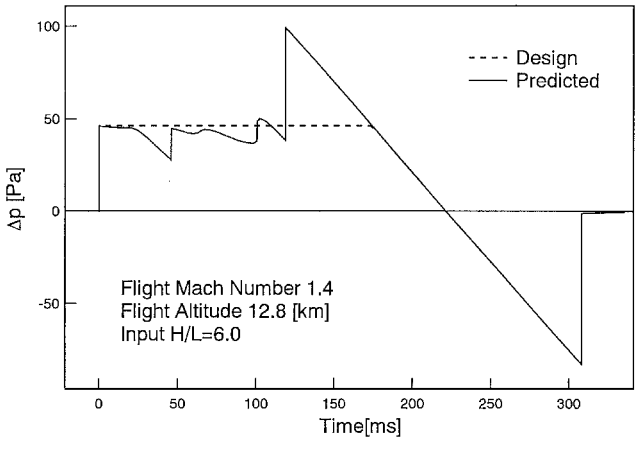

Fig. 7 Ground pressure signature.

respectively. The agreement between Volume + Lift and Designed is quite good. Therefore this low-boom aircraft is accurately designed in accordance with Darden's low-boom design method.

The waveform parameter method is used to extrapolate the near-field pressure signature to the ground. This method requires several input data such as aircraft flight conditions and atmospheric properties. The following input data are used here: flight Mach number of 1.4, flight altitude of 12.8 km, and standard no-wind atmospheric conditions. Figure 7 shows the extrapolated ground pressure signature for the low-boom configuration compared with the design signature. To include the three-dimensional effect of the aircraft, it is necessary to use a near-field pressure signature at some distance below the aircraft as input data of the waveform parameter method. In the case of this aircraft, the near-field pressure signature at a distance of $H/L = 6.0$ is used. The distance is determined by a preliminary sensitivity study. In Fig. 7, the predicted pressure signature shows a flattop shape in the front part and the initial peak pressure level is approximately 46 Pa, which is approximately the same as the initial design value of 42 Pa. However, there are significant discrepancies between the predicted ground pressure signature and the design signature, and the maximum pressure level in the predicted signature is approximately 100 Pa. One reason for these discrepancies is thought to be the three-dimensional effect of the aircraft configuration because the axisymmetrical nose of the aircraft achieves the flattop shape in the front part of the ground pressure signature.

Low-Boom Design Method by Use of Numerical Optimization

In this section, a new low-boom design method that couples the three-dimensional Euler CFD code and a least-squares optimization technique[12] is presented to modify the predicted ground pressure signature in Fig. 7.

The fuselage geometry of the aircraft is modified axisymmetrically in the optimization process to minimize the discrepancies between the calculated near-field pressure signature and the target signature. The axial distribution of radial perturbation is defined by a B-spline curve controlled by K points, whose radial coordinates δ_k are design variables in the optimization process.

The optimization method used in this study is based on a least-squares technique. The differences between the target and baseline pressures are reduced when perturbations are added to the baseline fuselage geometry iteratively. The object function to be minimized through the optimization is

$$J = \sum_{i=1}^{I} \left(P_{ti} - P_{bi} - \sum_{k=1}^{K} \frac{\partial P_i}{\partial \delta_k} \delta_k \right)^2 \Delta S_i \tag{3}$$

where the quantity $\partial P_i / \partial \delta_k$ is the response of the flowfield to the small radial perturbation δ_k. The unknown δ_k is to be determined by a least-squares method.

The target pressure signature is given in the near field of the aircraft. This target near-field pressure signature is determined so that the ground pressure signature extrapolated from it by the waveform parameter method becomes the target low-boom ground pressure signature.

Design Results

Some low-boom design examples are shown to validate this low-boom design method. Figure 8 shows an aircraft configuration that is used as an initial configuration for the validation. The aircraft has a 4.57-m-diam cylindrical fuselage with a sharp nose and a delta wing whose swept-back-angle is 77.5 deg. The profile of the delta wing is a 1.37-m-thick flat plate with the leading and the trailing edges with half angles of 10 deg.

In the validation, the low-boom pressure signatures shown in Fig. 2 are used as target ground pressure signatures. The flattop-type pressure signature is selected for case 1, the ramp type for case 2, and the hybrid type for case 3. The target near-field pressure signature for each case is defined at a distance of $H/L = 2.0$ below the aircraft so that the extrapolated ground pressure signature becomes the corresponding target low-boom ground pressure signature. The distance of $H/L = 2.0$ is determined to be the required location of the near field based on a preliminary sensitivity study for this simple aircraft configuration. The number of design variables represented by K, which is the number of controlling points for the B-spline curve, equals eight in these design examples. In these design processes, most of the computation time is consumed in the CFD analysis, because it is needed to calculate the flowfield $K + 1$ times in one optimization cycle to find flowfield responses to the geometry perturbations. Figure 9a shows the initial, the target, and the optimized near-field pressure signatures for case 1. The ground pressure signatures extrapolated from these are shown in Fig. 9b, and the optimized fuselage geometry and the initial geometry are shown in Fig. 9c. Similar figures for cases 2 and 3 corresponding to ramp and hybrid pressure signatures are shown in Figs. 10 and 11,

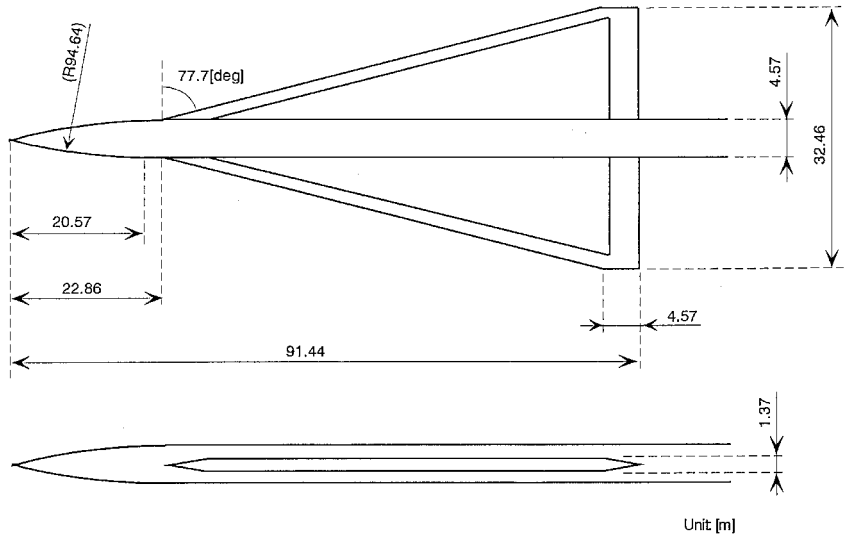

Fig. 8 Aircraft configuration for the validation of the low-boom design.

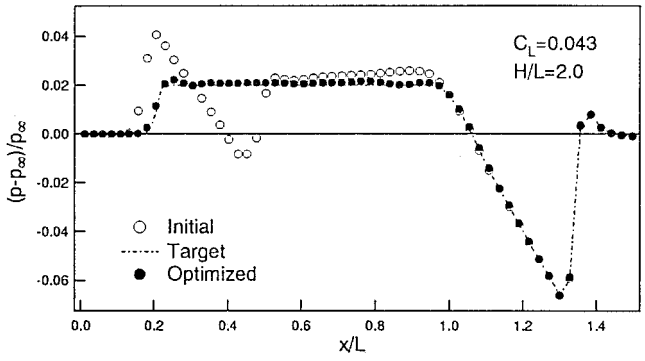

a) Near-field pressure signature

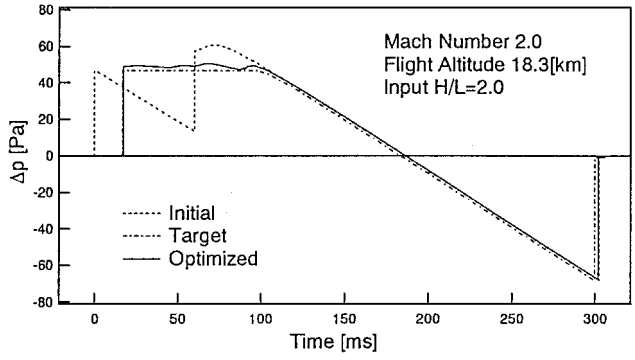

b) Ground pressure signature

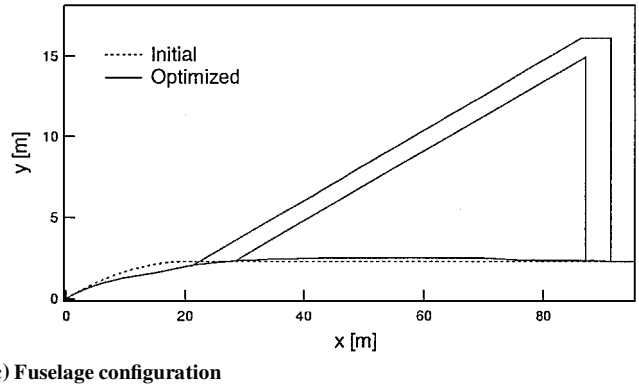

c) Fuselage configuration

Fig. 9 Low-boom design example: case 1, flattop-type low-boom pressure signature; M = 2.0.

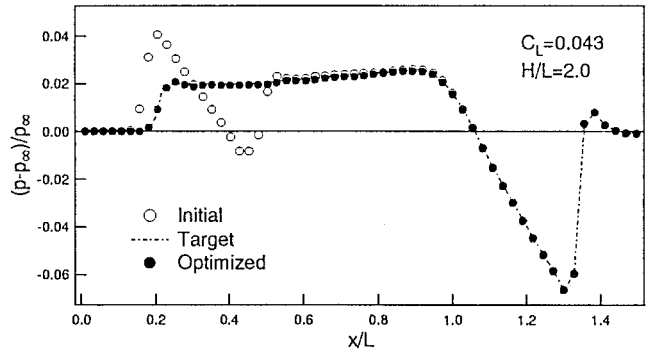

a) Near-field pressure signature

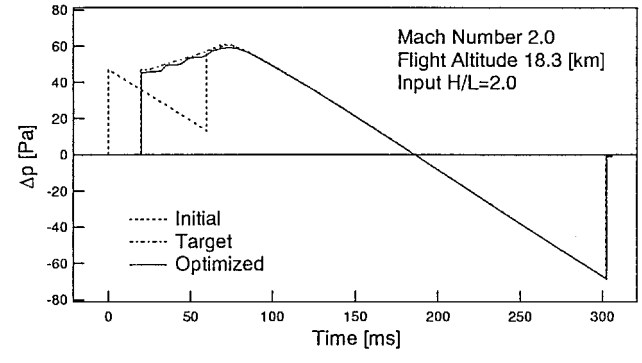

b) Ground pressure signature

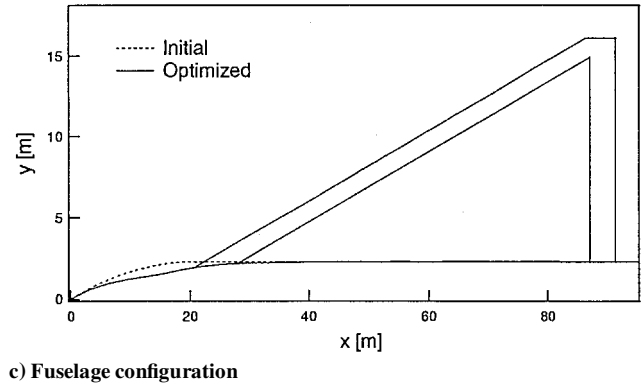

c) Fuselage configuration

Fig. 10 Low-boom design example: case 2, ramp-type low-boom pressure signature; M = 2.0.

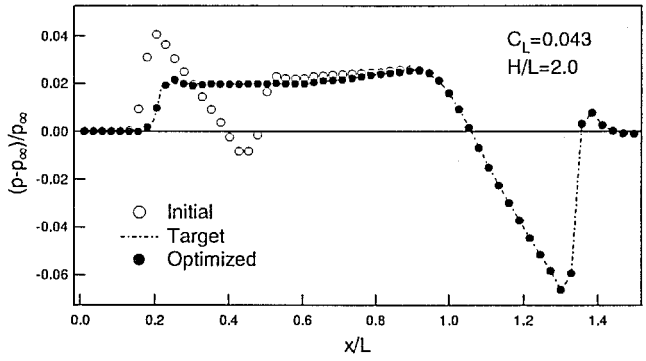

a) Near-field pressure signature

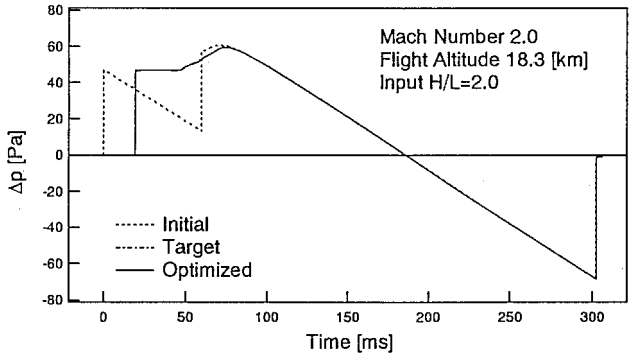

b) Ground pressure signature

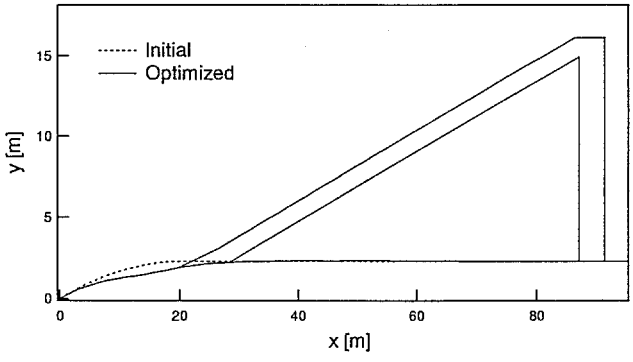

c) Fuselage configuration

Fig. 11 Low-boom design example: case 3, hybrid-type low-boom pressure signature; M = 2.0.

respectively. It is shown in these figures that optimized aircraft configurations can be developed that correspond to the target low-boom pressure signatures on the ground. These examples suggest that this design method is useful for low-boom design.

Next, the initial low-boom configuration shown in Fig. 3 is modified to generate a flattop-type pressure signature on the ground, shown in Fig. 7 (dashed line). The target pressure signature is given at a distance of $H/L = 6.0$ below the aircraft. The number of the controlling points for a B-spline curve is eight, and the range of the point distribution is changed as follows:

$$0.1 < x/L < 0.9 \qquad (1 \le N < 6)$$

$$0.1 < x/L < 0.6 \qquad (6 \le N < 9)$$

$$0.2 < x/L < 0.7 \qquad (9 \le N < 11)$$

$$0.3 < x/L < 0.8 \qquad (11 \le N < 13)$$

$$0.4 < x/L < 0.9 \qquad (13 \le N \le 14)$$

where N is the iteration number of the design cycle. In the first five cycles, the controlling points are distributed over the aircraft axis, except the axisymmetrical part of the configuration, and after

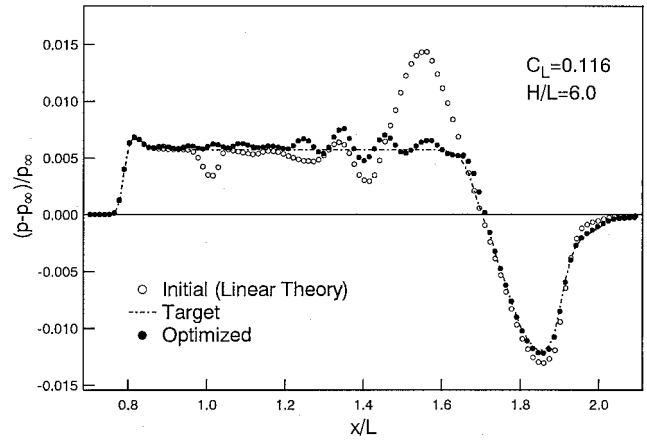

Fig. 12 Optimized near-field pressure signature at H/L = 6.0.

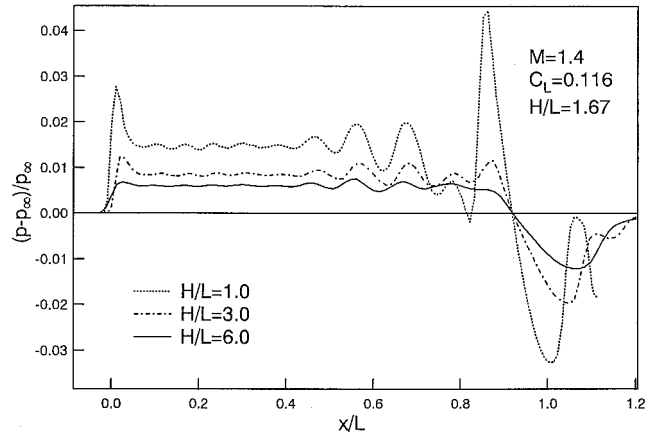

Fig. 13 Near-field pressure signatures for optimized low-boom configuration.

that they are distributed in narrower part of the axis for detailed modification of the fuselage geometry.

Figure 12 shows the optimized near-field pressure signature with the target and initial pressure signatures at $H/L = 6.0$. The figure shows that the optimized pressure signature is flatter than the initial signature and in better agreement with the target. Figure 13 shows the optimized pressure signatures at $H/L = 1.0$, 3.0, and 6.0 compared with Fig. 5. In the rear part of the signature at $H/L = 1.0$, the pressure level before the highest peak becomes lower than that of the initial signature. As the distance from the aircraft becomes large, the pressure peaks in the rear part coalesce and form a flattop shape.

Figure 14 shows the convergence history of the optimization process. A convergence parameter is defined as

$$CP = \left[\frac{\sum_{i=1}^{T} (P_{ti} - P_{bi})^2 \Delta S_i}{\sum_{i=1}^{T} \Delta S_i} \right]^{\frac{1}{2}} \tag{4}$$

It is noted that the differences between the target and the initial pressures are reduced by the optimization.

Figure 15 shows the ground pressure signatures extrapolated from the near-field pressure signatures at $H/L = 6.0$ in Fig. 12. Comparing the optimized and the initial pressure signatures, we see that the maximum peak pressure level drops from 100 to 60 Pa. Sonic-boom intensities have historically been defined by the levels of their peak overpressure for typical N-wave signatures. For low-boom pressure signatures, however, it is not a sufficiently accurate indicator of human response, and some other noise metric such as an A-weighted sound pressure level or perceived noise level is needed.[13] In Ref. 14, a loudness of 72 dBA or less is proposed as an acceptance criterion from an analysis of available human-response

Table 2 Sonic-boom intensities

Series	Initial, dBA	Target, dBA	Optimized, dBA
A	89.1	86.9	87.1
B	84.0	81.6	81.9
C	79.4	76.7	77.4

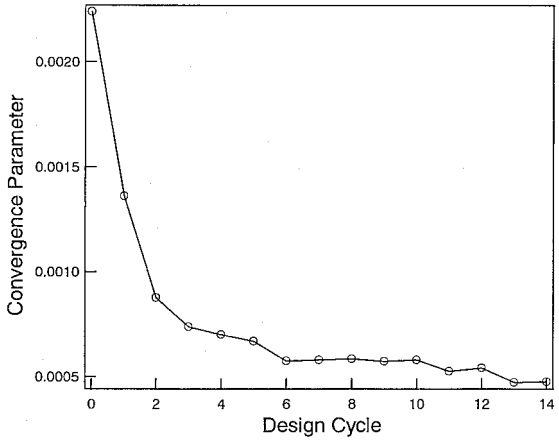

Fig. 14 Convergence history.

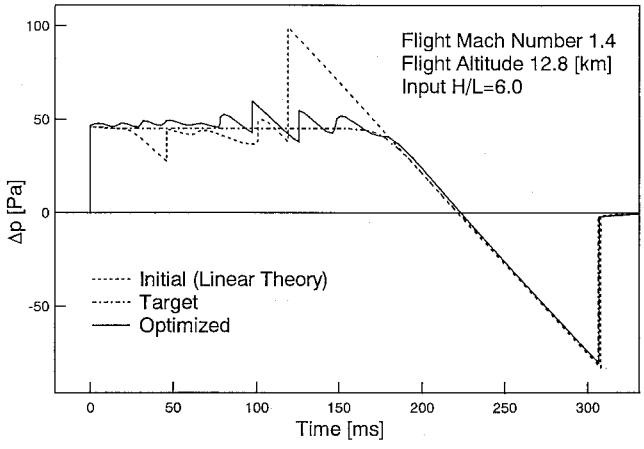

Fig. 15 Optimized ground pressure signature.

testing data. The sonic-boom intensities of the ground pressure signatures in Fig. 15 evaluated in terms of A-weighted decibels are shown in Table 2. The rise time of the shock overpressure in the ground pressure signature is predicted from the following empirical relations between the rise time ΔT_R and the shock overpressure Δp shown in Fig. 16:

$$\log \Delta T_R = A_1 \log \Delta p + A_2$$

$$\text{A-series: } A_1 = -0.923,\ A_2 = 1.88$$

$$\text{B-series: } A_1 = -0.920,\ A_2 = 2.23$$

$$\text{C-series: } A_1 = -1.080,\ A_2 = 2.79 \qquad (5)$$

The first approximate equation (A-series) is obtained from the molecular absorption theory.[15] The second (B-series) and third (C-series) equations are the empirical model and the outer boundary of the flight data,[16] respectively. The sonic-boom intensities of the target and the optimized ground pressure signatures evaluated in A-weighted decibels are approximately the same in all series, although there are a few discrepancies among these signatures, as shown in Fig. 15. The sonic-boom intensity of the optimized low-boom configuration is approximately 2 dBA smaller than that of the initial configuration in all series. The sonic-boom intensity of the optimized ground pressure signature, however, does not meet the loudness criteria of 72 dBA, even in the case of the C-series rise-time prediction. This is due to the tail shock pressure rise, which is approximalety 80 Pa. Additional modification of the tail configuration, including a tail wing, will be needed to reduce the shock pressure rise.

The optimized fuselage shown in Fig. 17 becomes wider in the rear part than the initial geometry because a strong expansion wave must be generated from the aircraft tail to reduce the pressure peak because of the shocks from the outer-wing leading edges. Because of this wider fuselage, the pressure drag coefficient

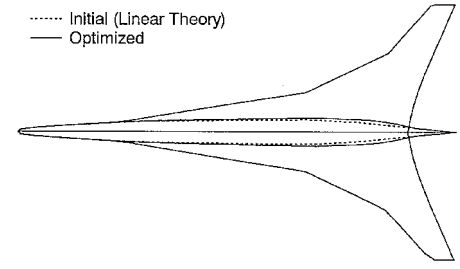

Fig. 17 Optimized fuselage geometry.

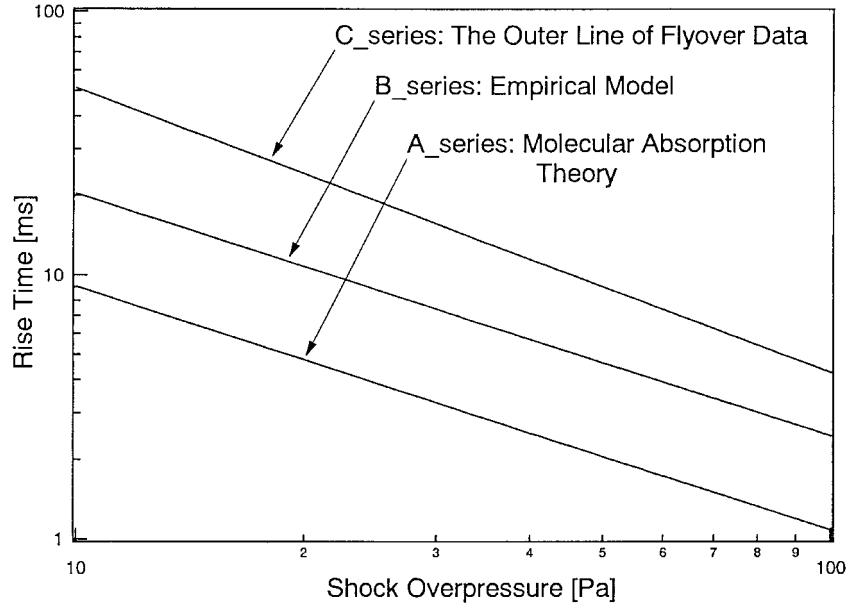

Fig. 16 Rise-time prediction.[16]

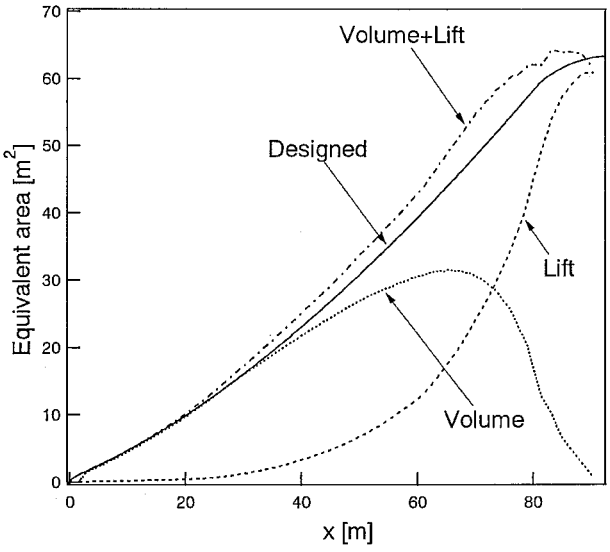

Fig. 18 Optimized equivalent-area distributions.

calculated from the CFD result of the optimized configuration becomes $C_{Dp} = 0.0121$, which is greater than that of the initial configuration of $C_{Dp} = 0.0103$. Some design constraints on fuselage volume or drag coefficient will be required in the optimization process.

Figure 18 shows the equivalent-area distribution of the optimized configuration compared with Fig. 6. The optimized distribution (Volume + Lift) is different from the designed distribution (Designed) because the actual area (Volume) of the optimized configuration becomes large in the tail part. The equivalent area that is due to the distribution of lift (Lift) does not change compared with that of Fig. 6 because only the fuselage geometry of the initial configuration is modified in the optimization. From the point of view of the aerodynamic performance, the optimization of the distribution of lift will be an important topic in low-boom design.

Conclusions

Aircraft configurations with minimized sonic-boom signatures are defined with the linear theory and a numerical optimization approach. The numerical low-boom design method combines a three-dimensional Euler CFD code with a least-squares optimization technique. It is shown that aircraft configurations that generate three types of low-boom pressure signatures, flattop type, ramp type, and hybrid type, can be successfully designed by this method. The fuselage geometry of the low-boom configuration designed by the linear theory is modified by the numerical optimization in order to minimize the pressure discrepancies between a target flattop-type low-boom signature and the calculated signature. The sonic-boom intensity of the optimized configuration is lower than that obtained from linear theory. Therefore it is suggested that this method is a useful tool for low-boom design. Further efforts will be required for the numerical low-boom design method for improving the sonic-boom acceptability and the aerodynamic performance of aircraft.

Acknowledgment

The authors express their sincere gratitude to Kawasaki Heavy Industries, Ltd., for providing the low-boom configuration.

References

[1] Whitham, G. B., "The Flow Pattern of a Supersonic Projectile," *Communications in Pure and Applied Mathematics*, Vol. 5, No. 3, 1952, pp. 301–348.

[2] Walkden, F., "The Shock Pattern of a Wing-Body Combination, Far from the Flight Path," *Aeronautical Quarterly*, Vol. 9, No. 2, 1957, pp. 164–194.

[3] Thomas, C. L., "Extrapolation of Sonic Boom Pressure Signatures by the Waveform Parameter Method," NASA TN D-6832, 1972.

[4] Siclari, M. J., and Darden, C. M., "Euler Code Prediction of Near-Field to Midfield Sonic Boom Pressure Signatures," *Journal of Aircraft*, Vol. 30, No. 6, 1993, pp. 911–917.

[5] Samson, H. C., Thomas, A. E., and Scott, L. L., "Application of Computational Fluid Dynamics to Sonic Boom Near- and Mid-Field Prediction," *Journal of Aircraft*, Vol. 29, No. 5, 1992, pp. 920–924.

[6] Seebass, R., and George, A. R., "Sonic-Boom Minimization," *Journal of the Acoustical Society of America*, Vol. 51, No. 2 (Pt. 3), 1972, pp. 686–694.

[7] Darden, C. M., "Sonic-Boom Minimization with Nose-Bluntness Relaxation," NASA TP-1348, 1979.

[8] Yoshida, K., "Experimental and Numerical Study for Aerodynamics of Low Boom Configuration," AIAA Paper 94-0052, 1994.

[9] Makino, Y., Sugiura, T., Watanuki, T., Kubota, H., Aoyama, T., and Iwamiya, T., "Effect of Nose Bluntness of a Low-Boom Configuration on Sonic-Boom," AIAA Paper 97-2213, June 1997.

[10] Chakravarthy, S. R., and Osher, S., "A New Class of High Accuracy TVD Schemes for Hyperbolic Conservation Laws," AIAA Paper 85-0363, Jan. 1985.

[11] Makino, Y., Sugiura, T., Kaido, A., Watanuki, T., Kubota, H., and Aoyama, T., "The Effect of the Body Configuration on the Sonic-Boom Intensity," AIAA Paper 96-2466, June 1996.

[12] Lee, D. K., and Eyi, S., "Aerodynamic Design via Optimization," *Journal of Aircraft*, Vol. 29, No. 6, 1992, pp. 1012–1019.

[13] Darden, C. M., Hayes, W. D., George, A. R., and Pierce, A. D., "Status of Sonic Boom Methodology and Understanding," *Proceedings of the Sonic-Boom Workshop*, NASA CP-3027, 1989.

[14] Haglund, G. T., "HSCT Design for Reduced Sonic Boom," AIAA Paper 91-3103, Sept. 1991.

[15] Pierce, A. D., "Relaxation and Turbulence Effects on Sonic-Boom Signatures," *High-Speed Research: Sonic-Boom*, NASA CP-3172, 1992.

[16] Darden, C. M., and Shields, E. W., "Elements of NASA's High-Speed Research Program," AIAA Paper 93-2942, July 1993.